ISSN (Print) 1226-1750
ISSN (Online) 2233-6656
Journal of Magnetics 25(4), 614-619 (2020) https://doi.org/10.4283/JMAG.2020.25.4.614

Energy Spectrum of Electromagnetic Radiation for a Dual-Energy Cone-Beam Computed Tomography in Radiotherapy

Seunghyeop Baek[1], Jin Sung Kim[2], Woo Sang Ahn[3]*, and Sohyun Ahn[2]*

[1]Department of Radiological Science, Yonsei University, Wonju 26493, Republic of Korea
[2]Department of Radiation Oncology, Yonsei University College of Medicine, Seoul 03722, Republic of Korea
[3]Department of Radiation Oncology, Gangneung Asan Hospital, University of Ulsan College of Medicine, Gangneung 25440, Republic of Korea

(Received 26 October 2020, Received in final form 29 Novemer 2020, Accepted 1 December 2020)

To implement dual-energy cone-beam computed tomography (CBCT), a 1 to 3 mm thick copper filter was applied in front of the kilovolt generator mounted on a medical linear accelerator. The energy calibration was performed from three energy peaks among the electromagnetic radiation, gamma rays, emitted by the ^{192}Ir source. The energy spectrum was measured using a cadmium zinc telluride (CZT) detector. A figure-of-merit (FOM) value was defined and evaluated in order to consider both the increase in the mean energy and the decrease in the intensity according to the filter. For a 1 mm thick filter, the FOM values were 0.82 and 0.92 for tube voltages of 100 and 120 kVp, respectively. The intensity was maintained reasonably and the effect of increasing the mean energy was evident, thus indicating its suitability for implementing dual-energy CBCT.

Keywords : electromagnetic spectrum, CZT detector, dual-energy CBCT, energy modulation filter, energy in electromagnetic radiation

1. Introduction

Computed tomography (CT) based on X-rays, which are electromagnetic waves with wavelengths in the range 0.01–10 nm, is important in radiation therapy (Fig. 1). A series of images are acquired by a CT scanner for planning radiation treatments [1, 2]. To identify a patient's set-up prior to the radiation treatment, cone-beam computed tomography (CBCT) imaging, which provides a set of three-dimensional (3D) volumetric images, is acquired using a flat-panel detector and a kilovolt (kV) X-ray source integrated into a linear accelerator. CBCT has been widely used as it plays an important role in image-guided radiation therapy [3, 4]. Recently, it was used to calculate dose distributions by directly using CBCT images to verify the dose provided to the tumors and organs at risk (OARs) and re-plan the treatment if necessary [5, 6]. This re-planning process is defined as adaptive radiation therapy.

*Co-corresponding author: Tel: +82-2-2228-4390
Fax: +82-504-158-4052, e-mail: mpsohyun@gmail.com
Tel: +82-33-610-5315, Fax: +82-33-610-5420
e-mail: anidol@ulsan.ac.kr

However, compared to CT images, CBCT has limitations such as non-uniformity and the presence of image artifacts due to scatter radiation and beam hardening [7-10]. To overcome these shortcomings, several researchers have developed various correction strategies according to the characteristics of the CBCT system and evaluated the reliability of dose calculation. The first strategy is to acquire the CBCT images of phantoms with inserts of

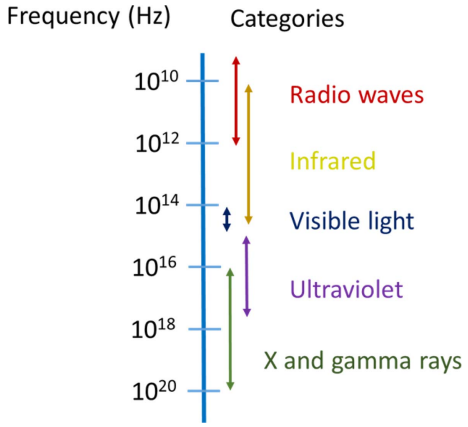

Fig. 1. (Color online) The major categories of electromagnetic waves as a function of frequency (Hz).

different densities and correct the voxel values corresponding to each material [11, 12]. The second strategy is to improve the image quality by directly measuring or simulating the scatter components of CBCT and then removing the scatter radiation from the raw projection data [13-15]. The third strategy is to map the Hounsfield unit (HU) value of the planning CT image to the CBCT image based on the rigid or deformable image registration method [16-18]. However, these methods are prone to dosimetric errors due to the presence of CBCT artifacts, and they have implementation limitations because scattered X-rays must be removed by all of the acquisition and scan conditions of CBCT. In addition, HU mapping is affected by geometric uncertainties related to image-registration errors.

One approach to improve soft-tissue visibility and CT number accuracy in CBCT is by employing dual-energy imaging. Since dual-energy CT can acquire information about relative electron density and effective atomic numbers, it can identify unique materials and provide quantitative information about them through CT images. According to the literature, it is generally possible to obtain dual-energy by means of rapid voltage switching, double-layer detection, and sequential acquisition [19, 20]. These methods have limitations that they either require two X-ray sources and two detectors or they can only obtain dual-energy limited to the maximum tube voltage.

In the previous study, to reduce the metal artifact and image contrast of CBCT, we designed an energy modulation filter to generate hardened beams with a higher mean energy in electromagnetic radiation, x-ray. As a result, when the modulation filter was used, the mean energy of the electromagnetic spectrum was effectively improved even at the same tube voltage. In this study, the mean energy of the energy spectra with varying thicknesses of a copper filter for dual-energy CBCT was measured using a cadmium zinc telluride (CZT) detector [21]. And the experimental results were compared with the MC results obtained in the previous study. The possibility of the application of ^{192}Ir, which is not a standard source generally used for energy-to-channel calibration of multichannel analyzer (MCA) was evaluated.

2. Materials and Methods

2.1. Energy-to-channel calibration

In this study, a CZT microspectrometer (microSpec500, Ritec) integrated with an MCA was used. The measurable energy range of this detector is 20 keV–3.0 MeV, and the number of channels of the MCA is up to 4k. The signal shaping time is 0.1–2 μs, with a 0.1 μs step. The detector consists of a base module and a detector module; the detector volume is 500 mm^3 and the external dimensions are 25 mm × 25 mm × 71 mm. The energy resolution of this detector is 2.5 % at 662 keV. A brachytherapy ^{192}Ir source from the Department of Radiation Oncology, Gangneung Asan Hospital, was used for energy-to-channel calibration. Table 1 lists the mean energy and intensity of the gamma rays emitted by the ^{192}Ir source.

Table 1. Gamma-ray spectrum of ^{192}Ir.

Group number	Mean energy (keV)	Intensity (%)
1	884.5	0.3
2	612.5	5.4
3	604.4	8.2
4	588.6	4.5
5	468.1	47.8
6	316.5	82.9
7	308.5	29.7
8	296.0	28.7
9	136.4	0.2

National Nuclear Data Center, Brookhaven National Laboratory, https://www.nndc.bnl.gov/nudat2/decaysearchdirect.jsp?nuc=192IR&unc=nds

The remote afterloading device used in the experiment was a microSelectron® developed by Nucletron (Fig. 2). The activity of the ^{192}Ir source on the day of the experiment was 7.79 Ci, and the number of MCA channels was 2048. After measuring the energy spectrum, energy peaks (316.5 keV, 468.1 keV, and 604.4 keV) with relatively high intensity among the ^{192}Ir gamma rays, were used for the energy calibration. This calibration allows the conversion of the x-axis channel numbers into energy values in kiloelectronvolt with the following equation:

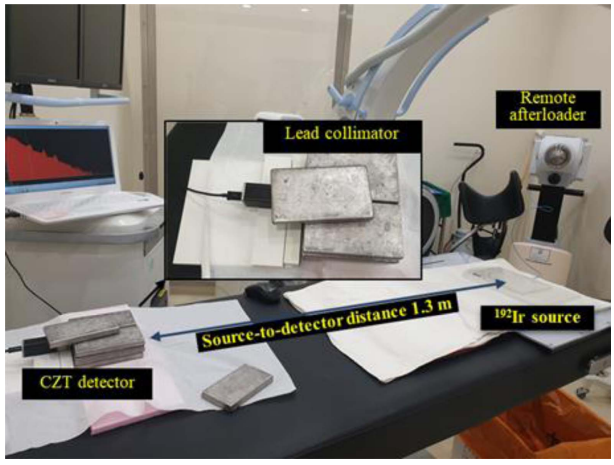

Fig. 2. (Color online) Experimental set-up to measure the energy spectrum of the ^{192}Ir source for energy calibration.

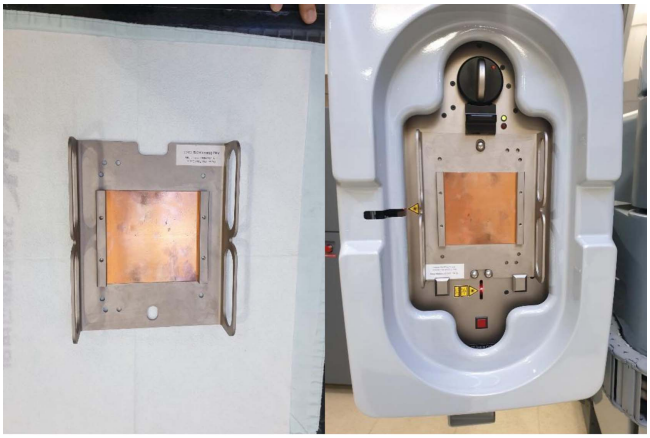

(a) (b)

Fig. 3. (Color online) A copper filter (a) and kV X-ray generator (b) for dual-energy modulation.

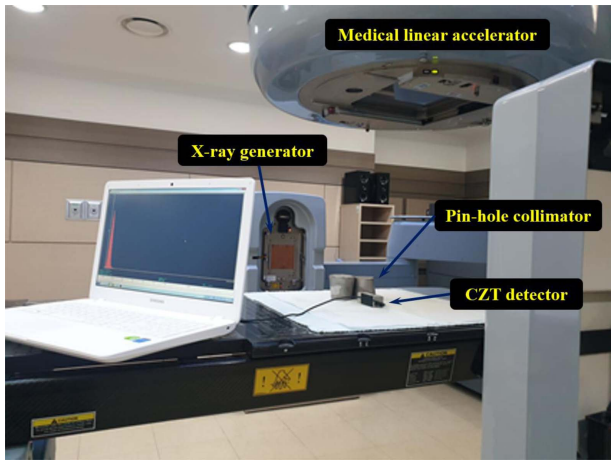

Fig. 4. (Color online) Experimental set-up to measure the energy spectrum of the kV X-ray source.

$$E_r = S \times C(channels) + O, \quad (1)$$

where S and O are the slope and intercept of the calibration line, respectively, and C is the channel number. The coefficients can be set by the linear fit of two energy channels/peak centroid pairs. To prevent overflow when measuring the energy spectrum, the distance between the source and detector was set at 1.3 m.

2.2. Measurement of the energy spectrum

An energy modulation filter of thickness of 1–3 mm was used considering the results of a previous MC simulation study [20]. To apply the energy modulation filter to the treatment equipment, the filter was attached to the front of the kV X-ray generator using the frame of the existing bowtie filter (Fig. 3). Cone-beam CT acquires images while rotating the gantry 360 degrees. However, the detector must face the X-ray generator while continuously rotating 360 degrees in order to measure the energy spectrum, and it is not easy to set up this experiment. Therefore, in this experiment, the gantry was fixed at one angle and then the energy spectrum was measured (Fig. 4). Four tube voltages, 60, 80, 100, and 120 kVp, which are the most commonly used in cancer treatment, were measured. To quantitatively evaluate the change in intensity, the experiment was conducted while maintaining a constant tube current (10 mA) and delivery time (3 min). For each tube voltage, the energy spectrum measurement was repeated four times while changing the condition from filterless to 1–3 mm filters, and the number of channels of the MCA was set to 2048. The mean energy and intensity of the energy spectrum measured for each condition were compared. The signal observed in the channel above the maximum energy for each tube voltage was due to coincidence signals; therefore, it was excluded from the analysis. In addition, to analyze the optimized filter thickness for each tube voltage after considering the mean energy and intensity, the figure of merit (FOM) was defined as follows:

$$FOM = R_{mean\ energy} \times R_{intensity}, \quad (2)$$

where $R_{mean\ energy}$ is the ratio of the mean energy with the filter to the mean energy without the filter, and $R_{intensity}$ is the ratio of the intensity with the filter to the intensity without the filter.

3. Results

3.1. Energy-to-channel calibration

Figure 5 shows the measured energy spectrum of ^{192}Ir. As listed in Table 1, the peak (A) with the highest intensity is 316.5 keV (82.9 %), and the centroid channel

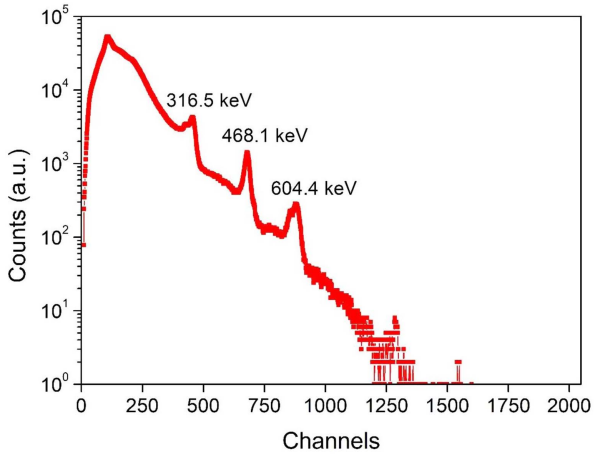

Fig. 5. (Color online) Measured energy spectrum of ^{192}Ir source.

Table 2. Mean energies of the energy spectra according to the filter thicknesses (unit: keV).

Tube voltage (kVp)	Thickness of copper filter					
	w/o filter	w/o filter*	1 mm	2 mm	2 mm*	3 mm
60	33.1	-	41.3	38.7	-	33.3
80	37.6	37.5	52.0	52.8	62.7	49.4
100	41.4	-	60.6	66.0	-	64.9
120	49.1	56.2	64.6	71.1	85.4	72.6

*Simulation results from a previous research.

is 452. The second-highest intensity (B) peak corresponds to 468.1 keV (47.8 %) and the centroid channel is 680. The third-highest intensity (C) peak is 604.4 keV (8.2 %) and the centroid channel is 880. Using the three peaks, the following energy-to-channel calibration equation is obtained:

$$E\ [keV] = 0.66 \times Channels + 19.68 \quad (3)$$

3.2. Measurement of energy spectrum

Table 2 shows the results of the mean energy analysis after measuring the energy spectrum while changing the thickness of the energy modulation filter in the kV X-ray generator attached to the radiation therapy equipment. At 60 kVp with a 1 mm filter, the mean energy was similar to that at 100 kVp. However, when the thickness of the filter was increased to 2 or 3 mm, the mean energy decreased, which is believed to be due to the increasing influence of the characteristic X-ray spectrum of copper. At 80 kVp with the 1 mm filter, the mean energy, 52.0 keV, was found to be higher than that obtained without a filter, 49.1 keV, at 120 kVp. In addition, when the 2 and 3 mm filters were used, the mean energies were 52.8 and 49.4 keV, respectively, which are not significantly different from the mean energy obtained using the 1 mm filter (52.0 keV).

In the simulation results of the previous study listed in Table 1, at 80 kVp, the mean energy was 37.5 keV without the filter, which is close to the measured mean energy of 37.6 keV. When the 2 mm filter was applied, the mean energy was 62.7 keV in the simulation results; however, the measured mean energy was 52.8 keV, thus indicating a difference between simulation and measurement.

At 100 kVp with the 1 and 2 mm filters, the mean energy increased to 60.6 and 66.0 keV, respectively. With the 3 mm filter, the mean energy, 64.9 keV, decreased compared to that obtained using the 2 mm filter. At 120 kVp, the mean energy continuously increased with the thickness of the filter, and no reversal phenomenon in the tube voltage range of 60–100 kVp occurred. The simulation results for 120 kVp also showed a higher mean energy compared to the measurement results, which is similar to the simulation result for 80 kVp.

Table 3. Relative intensities of energy spectra according to the filter thicknesses (unit: %).

Tube voltage (kVp)	Thickness of copper filter			
	w/o filter	1 mm	2 mm	3 mm
60	100.0	5.8	1.2	0.7
80	100.0	8.2	2.3	1.2
100	100.0	55.7	22.3	5.7
120	100.0	69.7	45.7	15.7

Table 3 shows the relative intensity of the energy spectrum. For 60 kVp, the intensity with the 1 mm filter is only 5.8 % compared to the filterless case. Since the noise in an image is closely related to the intensity, the 1mm thick filter requires approximately 17.2 times the output (tube current) or lengthens the image acquisition time in order to derive the same image noise as without the filter. At 80 kVp, 8.2 % of relative intensity was obtained using the 1 mm filter compared to that in the filterless case, which indicates that 12.2 times the output or an equivalent image acquisition time was required. At 100 kVp, 55.7 % of the relative intensity was obtained using the 1 mm filter compared to that in the filterless case, indicating that approximately 1.8 times the output is required. At 120 kVp, when using the 1 mm filter, the relative intensity decreased to 69.7 % compared to that in the filterless case, and when using 2 and 3 mm, the relative intensities decreased to 45.7 % and 15.7 %,

Table 4. FOMs of energy spectra according to the filter thicknesses.

Tube voltage (kVp)	Thickness of copper filter		
	1 mm	2 mm	3 mm
60	0.07	0.01	0.01
80	0.11	0.03	0.02
100	0.82	0.36	0.09
120	0.92	0.66	0.23

respectively.

Table 4 shows the results of the FOM values considering the mean energy and intensity of each energy spectrum. For a tube voltage of 120 kVp with the 1 and 2 mm filters, the FOMs are 0.92 and 0.66, respectively, and this intensity can be used to increase the mean energy efficiently. At 100 kVp, the FOM is 0.82 with the 1 mm filter and 0.36 and 0.09 with the 2 and 3 mm filters, respectively. In contrast, for 60 and 80 kVp, the FOM is < 0.11 for all the filter thicknesses, which is inadequate compared to 100 and 120 kVp in terms of mean energy and intensity efficiency.

4. Discussion

The ^{192}Ir source used for the energy calibration in this study emits gamma rays of lower energy than ^{137}Cs (662 keV), which is a standard source mainly used for energy calibration. The energy range of the gamma rays emitted by a ^{192}Ir source is closer to the energy of CBCT as compared to a ^{137}Cs source. Also, ^{192}Ir source is widely used in clinical environments, particularly in the department of radiation oncology. In addition, its half-life (74 days) is adequate and it has good accessibility. Therefore, it has sufficient potential as a novel standard source. Moreover, more than three energy peaks were clearly observed in the experiments of this study and ^{192}Ir source was chosen as one candidate source for accurate energy calibration. However, since ^{192}Ir has been used as a source in brachytherapy applied directly to the tumor by a sealed source, its activity is stronger than different energy calibration sources. To prevent overflow in the detector, measures such as a pin-hole collimator or a sufficient distance between the source and the detector were required.

The CZT detector used in this study can be used at room temperature as an integrated MCA type; however, it has a disadvantage that it provides a medium resolution compared to a high-purity germanium detector, which has a high resolution. In other words, its energy resolution is 2.5 % in the energy range of 662 keV; therefore, it is not possible to discriminate differences at energies < 16.6 keV. Among the gamma-ray energies emitted from ^{192}Ir as shown in Table 1, it was verified that 296.0 keV, 308.5 keV, and 316.5 keV cannot be distinguished in the energy spectrum of ^{192}Ir shown in Fig. 5. Similarly, 588.6 keV, 604.4 keV, and 612.5 keV also cannot be distinguished. However, since the centroid channel of the peak would appear at the energy with the highest intensity, energy calibration is possible. Therefore, CZT is a useful detector in environments that do not provide a dedicated laboratory or nitrogen cooling system, such as hospitals.

Since the energy spectrum of an X-ray source in a kV CBCT rotating 360° of the linear accelerator is difficult to set up for measurement, we measured it in the fluoroscopy mode rather than the CBCT mode. The CBCT mode will be used when taking images for further study.

An energy modulation filter increases the mean energy of the energy spectrum by reducing the intensity of low-energy X-rays. This also means that the use of a filter leads to a decrease in intensity. The intensity in the image quality is closely related to the standard deviation (SD) which is an important parameter of the contrast-to-noise ratio (CNR) in Eq. (4):

$$CNR = \frac{\left|mean_a - mean_b\right|}{\sqrt{SD_a^2 + SD_b^2}}, \tag{4}$$

where $mean_a$ and $mean_b$ are the mean gray values in the areas a and b. SD_a and SD_b are the standard deviation of gray-values, respectively.

The influence of intensity reduction should also be considered as the mean energy enhanced by the energy modulation filter. In this study, a FOM was proposed in order to optimize the mean energy enhancement and the intensity reduction. Although it is a useful value at the current research stage, it has been determined that the FOM should be redefined in the future, including quantitative analysis on the quality of the image applied with an energy modulation filter. In addition, since the proposed method reduces the intensity of low-energy X-rays, it can be inferred that it will reduce the unnecessary imaging dose for patients; this will be evaluated experimentally in the future.

5. Conclusion

In this study, the possibility of effectively performing energy calibration using a ^{192}Ir source, which is widely used for brachytherapy in radiation oncology, was verified. In addition, a dual-energy spectrum generated with one source by controlling the mean energy using an energy modulation filter made of copper was realized. Furthermore, an appropriate filter thickness could be set to ensure the intensity reduction. In further study, a FOM should be redefined including quantitative analysis on the quality of the image applied with an energy modulation filter. Also, we will evaluate the reducing unnecessary imaging dose for patients through experiments.

Acknowledgments

This work was supported by the National Research Foundation of Korea (NRF) grant funded by the Korea

government (MSIT) (No. 2019R1A2C108912912) and Basic Science Research Program through the national research foundation of Korea (NRF) funded by the Ministry of Education (NRF-2018R1D1A1B07050217).

References

[1] P. Hobday, N. J. Hodson, J. Husband, R. P. Parker, and J. S. Macdonald, Radiology **133**, 177 (1979).
[2] J. J. Battista, W. D. Rider, and J. Van Dyk, Int. J. Radiat. Oncol. Biol. Phys. **6**, 99 (1980).
[3] D. A. Jaffray, J. H. Siewerdsen, J. W. Wong, and A. V. Martinez, Int. J. Radiat. Oncol. Biol. Phys. **53**, 1337 (2002).
[4] K. Nakagawa, H. Yamashita, H. Igaki, A. Terahara, K. Shiraishi, and K. Yoda, Radiat. Med. **26**, 570 (2008).
[5] G. Amit and T. G. Purdie, Med. Phys. **42**, 770 (2015).
[6] T. Almatani, R. P. Hugtenburg, R. D. Lewis, S. E. Barley, and M. A. Edwards, Br. J. Radiol. **89**, 1066 (2016).
[7] J. H. Siewerdsen and D. A. Jaffray, Med. Phys. **28**, 220 (2001).
[8] M. B. Sharpe, D. J. Moseley, T. G. Purdie, M. Islam, J. H. Siewerdsen, and D. A. Jaffray, Med. Phys. **33**, 136 (2006).
[9] K. Srinivasan, M. Mohammadi, and J. Shepherd, Pol. J. Radiol. **79**, 181 (2014).
[10] W. Zhao, D. Vernekohl, J. Zhu, L. Wang, and L. Xing, Med. Phys. **43**, 1736 (2016).
[11] A. Richter, Q. Hu, D. Steglich, K. Baier, J. Wilbert, M. Guckenberger, and M. Flentje, Radiat. Oncol. **3**, 42 (2008).
[12] Y. Rong, J. Smilowitz, D. Tewatia, W. A. Tomé, and B. Paliwal, Med. Dosim. **35**, 195 (2010).
[13] L. Zhu, Y. Xie, J. Wang, and L. Xing, Med. Phys. **36**, 2258 (2009).
[14] G. Poludniowski, P. M. Evans, V. N. Hansen, and S. Webb, Phys. Med. Biol. **54**, 3847 (2009).
[15] M. Skaarup, J. M. Edmund, S. Dorn, M. Kachelriess, and I. R. Vogelius, Acta Oncologica. **58**, 1483 (2019).
[16] M. V. Zijtveld, M. Dirkx, and B. Heijmen, Radiother. Oncol. **85**, 195 (2007).
[17] Y. Yang, E. Schreibmann, T. Li, C. Wang, and L. Xing, Phys. Med. Biol. **52**, 685 (2007).
[18] Y. Onozato, N. Kadoya, Y. Fujita, K. Arai, S. Dobashi, K. Takeda, K. Kishi, R. Umezawa, H. Matsushita, and K. Jingu, Int. J. Radiat. Oncol. Biol. Phys. **89**, 416 (2014).
[19] T. Johnson, C. Fink, S. O. Schonberg, and M. F. Reiser, Dual Energy CT in Clinical Practice. Springer (2011).
[20] T. P. Szczykutowicz and G.-H. Chen, Phys. Med. Biol. **55**, 6411 (2010).
[21] Y. Kim, T. Lee, and W. Lee, NET **51**, 1417 (2019).
[22] S. Ahn, S. J. Cho, K. C. Keum, S. G. Choi, and R. Lee, Prog. Med. Phys. **27**, 8 (2016).